Ganji et al., *BioImpacts.* 2023;13(6):505-520
doi: 10.34172/bi.2023.26456
https://bi.tbzmed.ac.ir/

# Epithelial cells/progenitor cells in developing human lower respiratory tract: Characterization and transplantation to rat model of pulmonary injury

**Fatemeh Ganji[1,2], Marzieh Ebrahimi[3], Ali Shirani[1,2], Mahtab Golmohammadi[4], Mazaher Gholipourmalekabadi[1,2], Maryam Kashanian[5], Kiana Koolaeinezhad[5], Hamid Reza Davari[6], Seyed Ali Javad Mousavi[7], Hamid Reza Aghayan[8], Babak Arjmand[8,9], Ramin Heshmat[10], Nushin Karkuki Osguei[11], Ali Samadikuchaksaraei[12*]**

[1]Cellular and Molecular Research Center, Iran University of Medical Sciences, Tehran, Iran
[2]Department of Tissue Engineering & Regenerative Medicine, Iran University of Medical Sciences, Tehran, Iran
[3]Department of Stem Cells and Developmental Biology, Cell Science Research Center, Royan Institute for Stem Cell Biology and Technology, ACECR, Tehran, Iran
[4]Department of Genetic, Shahid Sadoughi University of Medical Sciences, Yazd, Iran
[5]Shahid-Akbarabadi Clinical Research Development Unit, Iran University of Medical Sciences, Tehran, Iran
[6]Thorax Advanced Research Center, Tehran University of Medical Sciences, Tehran, Iran
[7]Section of Respiratory Diseases, Department of Internal Medicine, Iran University of Medical Sciences, Tehran, Iran
[8]Cell Therapy and Regenerative Medicine Research Center, Endocrinology and Metabolism Molecular-Cellular. Sciences Institute, Tehran University of Medical Sciences, Tehran, Iran
[9]Metabolomics and Genomics Research Center, Endocrinology and Metabolism Molecular-Cellular Sciences Institute, Tehran University of Medical Sciences, Tehran, Iran
[10]Chronic Diseases Research Center, Tehran University of Medical Sciences, Tehran, Iran
[11]Eposcience Millennium Institute, Tehran, Iran
[12]Department of Medical Biotechnology, Iran University of Medical Sciences, Tehran, Iran

**Article Info**

***Article Type:***
Original Article

***Article History:***
Received: 14 May 2022
Revised: 12 Jan. 2023
Accepted: 30 Jan. 2023
ePublished: 22 July 2023

***Keywords:***
Fetal stem cells
Fetus
Organoids
Lung
Bronchi

**Abstract**

***Introduction:*** For cell-based therapies of lung injury, several cell sources have been extensively studied. However, the potential of human fetal respiratory cells has not been systematically explored for this purpose. Here, we hypothesize that these cells could be one of the top sources and hence, we extensively updated the definition of their phenotype.

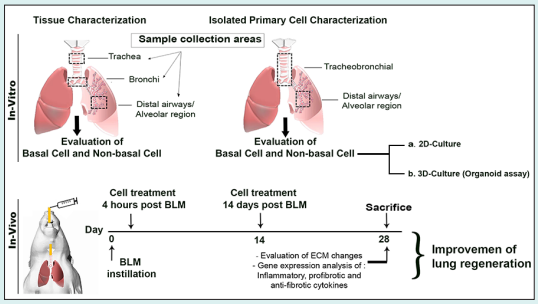


***Methods:*** Human fetal lower respiratory tissues from pseudoglandular and canalicular stages and their isolated epithelial cells were evaluated by immunostaining, electron microscopy, flow cytometry, organoid assay, and gene expression studies. The regenerative potential of the isolated cells has been evaluated in a rat model of bleomycin-induced pulmonary injury by tracheal instillation on days 0 and 14 after injury and harvest of the lungs on day 28.

***Results:*** We determined the relative and temporal, and spatial pattern of expression of markers of basal (KRT5, KRT14, TRP63), non-basal (AQP3 and pro-SFTPC), and early progenitor (NKX2.1, SOX2, SOX9) cells. Also, we showed the potential of respiratory-derived cells to contribute to *in vitro* formation of alveolar and airway-like structures in organoids. Cell therapy decreased fibrosis formation in rat lungs and improved the alveolar structures. It also upregulated the expression of *IL-10* (up to 17.22 folds) and surfactant protein C (up to 2.71 folds) and downregulated the expression of *TGF-β* (up to 5.89 folds) and *AQP5* (up to 3.28 folds).

***Conclusion:*** We provide substantial evidence that human fetal respiratory tract cells can improve the regenerative process after lung injury. Also, our extensive characterization provides an updated phenotypic profile of these cells.

*Corresponding author: Ali Samadikuchaksaraei, Email: samadikuchaksaraei@yahoo.com, ali.samadi@iums.ac.ir

## Introduction

Cell therapy for lung injury has been the subject of extensive research, and several cells have been studied as potential sources.[1,2] However, the potential of the fetal respiratory tract cells, which are naturally developing in their native niche, has not been systematically studied for the cells derived from human tissues.

Obviously, the successful completion of such a study necessitates an up-to-date understanding of the step-wise events, cellular differentiation, and temporal and spatial changes in gene expression during human lower respiratory tract development. Unfortunately, compared to reports on the characterization of the epithelial cells/progenitor cells in rodent's respiratory system, much less has been studied in humans. There are numerous pieces of evidence showing that the development of respiratory epithelium in humans and rodents do not follow an exact pattern.[3,4] Our current knowledge in human respiratory development is based on reports of direct tissue examination[5] and in vitro culture of human samples.[6,7] Still, these data do not provide a complete phenotypic profile of cellular components of the respiratory tract during human fetal development. The signaling pathways, that control the undifferentiated/differentiated status of respiratory stem cells during the stages of development, might be recruited during the process of repair and regeneration[8], which necessitates their detailed elucidation.

Currently, bleomycin-induced injury in rodents is one of the most studied models for evaluating the effects of cell therapy on lung injury. Most of these studies have focused on applying mesenchymal stem cells for cell-based therapies.[9] However, these cells are most effective when administered during the early inflammatory phase after injury.[10] The regenerative potential of other cell sources has been reported to differ in several aspects. For instance, alveolar type II cell therapy was reported to be effective even during the late inflammatory phase after injury.[11] Another example is the report showing that term human amniotic epithelial cells lead to better pulmonary regeneration than preterm cells.[12]

Here, we hypothesize that human fetal respiratory tract cells could be one of the top choices on the list for cell therapy for lung injury. In this study, we show that fetal lower respiratory tract-derived cells improve the process of regeneration during both early and late phases after experimental lung injury. Also, to have an updated phenotypic profile, we extensively characterize the epithelial cells/progenitor cells throughout the human fetal lower respiratory tract in both pseudoglandular and canalicular stages.

## Materials and Methods

### *Sample collection and study design*

Fetal lower respiratory tract tissues were obtained from cadaveric fetuses following spontaneous abortion, and legal termination of pregnancy for severe fetal neurological anomaly and severe maternal cardiac disease (Table 1). Fetuses from mothers older than 40 years of age and from mothers with diabetes, hormonal disorders, viral and parasitic infections, and pulmonary disorders were not included in the study. Also, fetuses with cardiac and pulmonary disorders and those aborted following ectopic pregnancy were excluded. Tissues procured from 20 fetuses were examined. The accuracy of the age of each fetus was determined by the Hern's guideline using physical measurements.[13] Ages of fetuses ranged from 12–19 weeks of gestation, which corresponded to pseudoglandular and canalicular stages (Table 1)[14] (10 respiratory tissues were examined for each stage). A 2 × 2 cm human adult healthy lung tissue was obtained from a 63 years old patient who underwent open lung biopsy in Rasoul Akram Hospital (Tehran, Iran) for diagnosis of idiopathic pulmonary fibrosis (IPF). The patient presented with the clinical features of exertional dyspnea, dry cough, decreased total lung capacity (TLC) and decreased forced vital capacity (FVC). But, histopathological examination showed normal histological features.

After dissection of heart and lower respiratory tract tissues, all tissue samples were placed in a 4 °C DMEM/F12 culture medium (Sigma, Missouri, USA), 10% Fetal Bovine Serum (FBS, Gibco, Gaithersburg, USA), and 0.5% (v/v) antibiotic/antimycotic (10 000 units/mL of penicillin, 10 000 µg/mL of streptomycin, and 25 µg/mL of fungizone) (Gibco, Gaithersburg, USA). The samples were then promptly delivered to the laboratory. Fetal respiratory tissue samples were divided and cut into three anatomical regions including: trachea, bronchi, and distal airways/alveolar region for histological examination. Also, mixed cell populations were isolated from two anatomical regions of tracheobronchial and distal airways/alveolar, and were subjected to phenotypic and molecular characterizations.

### *Histological evaluations*

Freshly dissected tissue samples were fixed in 4% (w/v) formaldehyde in double distilled water at 4 °C for 48 hours. Then, all samples were dehydrated through a graded series of ethanol solutions (50%, 70%, 80%, 90%, and 100%; 1 hour each), paraffin-embedded, and sectioned at 6 µm thickness slices. The slides were deparaffinized and rehydrated for H&E and Masson trichrome, immunostaining.

### *Immunochemical staining of tissue samples*

For immunostaining, an antigen retrieval process was performed with 10 mM sodium citrate buffer (pH 6.0) (20 minutes at 120 °C) and the samples were permeabilized with 0.5% Triton-X100 at room temperature (15 minutes). The sections were blocked with 10% goat serum in PBS at 37 °C (1 hour). Primary antibodies were diluted in 5% goat serum. The sections were treated overnight at 4 °C with primary antibodies including 1:50, mouse anti-pan-Keratin (Thermo Fisher Scientific, Waltham, Massachusetts, USA); 1:250, rabbit anti-KRT5; 1:100,

Table 1. Details of fetuses included in this study

| Code number | Gestational age (wk) | Lung developmental stage | Cause of abortion |
|---|---|---|---|
| 1 | 12 | Pseudoglandular | SAB |
| 2 | 12 | Pseudoglandular | SAB |
| 3 | 14 | Pseudoglandular | LTP for severe fetal neurological anomaly |
| 4 | 14 | Pseudoglandular | SAB |
| 5 | 14 | Pseudoglandular | LTP for severe maternal cardiac disease |
| 6 | 15 | Pseudoglandular | SAB |
| 7 | 15 | Pseudoglandular | LTP for severe maternal cardiac disease |
| 8 | 15 | Pseudoglandular | LTP for severe fetal neurological anomaly |
| 9 | 16 | Pseudoglandular | SAB |
| 10 | 16 | Pseudoglandular | LTP for severe fetal neurological anomaly |
| 11 | 17 | Canalicular | SAB |
| 12 | 17 | Canalicular | SAB |
| 13 | 17 | Canalicular | LTP for severe fetal neurological anomaly |
| 14 | 18 | Canalicular | LTP for severe maternal cardiac disease |
| 15 | 18 | Canalicular | SAB |
| 16 | 18 | Canalicular | SAB |
| 17 | 18 | Canalicular | SAB |
| 18 | 19 | Canalicular | LTP for severe fetal neurological anomaly |
| 19 | 19 | Canalicular | SAB |
| 20 | 19 | Canalicular | LTP for severe fetal neurological anomaly |

SAB: spontaneous abortion; LTP: legal termination of pregnancy

mouse anti-KRT14; 1:200, mouse anti-Trp63; 1:250, rabbit anti-AQP3; 1:250, rabbit anti-AQP5; and 1:500, rabbit anti-pro-SFTPC (all from Abcam, Cambridge, USA) (anti-pan-Keratin for epithelial cells; anti-KRT5, anti-KRT14 and anti-Trp63 for basal cells; anti-AQP3, anti-AQP5 and anti-pro-SFTPC mainly for non-basal cells). The samples were washed three times with phosphate-buffered saline (PBS), and then incubated for 1 hour at 37 °C with secondary antibodies including 1:1000, anti-Mouse Alexa Fluor 594; 1:1000, anti-Rabbit Alexa Fluor 594; and 1:1000, anti-Rabbit Alexa Fluor 488 (all from Abcam, Cambridge, USA). After double washing with PBS, the nuclei were counterstained for 1 min with DAPI (Sigma-Aldrich, St. Louis, USA). ImageJ software was used for counting the number of marker-positive cells in each micrograph.

Primary antibodies of KRT5, KRT14, Trp63, AQP3, AQP5 and pro-SFTPC were validated using positive and negative samples Fig. 1A. For human fetal samples, 6 sections of each region were stained and scored for each marker. Then, to quantify immunostaining results, each section was divided into 4 fields (24 fields/sample) and cells were counted using ImageJ software.

### *Electron microscopy and ultrastructural analysis*

Tissues were fixed in 2.5% glutaraldehyde (Sigma-Aldrich, St. Louis, USA) at 4°C (72 hours), followed by post-fixation in 1% osmium tetroxide (Sigma-Aldrich, St. Louis, USA) (30 minutes). The samples were then dehydrated through a graded series of acetone solutions (30%, 50%, 70%, 90%, and 100%, 1 hour each) and gradually embedded in resin (Taab embedding resin, T027/1, UK). The resin blocks were sectioned into 50 nm-thick sections. The samples were observed under an HT7800 transmission electron microscope (Hitachi, Germany).

### *Real time RT-PCR*

The relative gene expression levels of molecular markers of early progenitor (*NKX2.1*, *SOX2, SOX9)* cells were measured for tracheobronchial and distal airways/alveolar regions for both pseudoglandular and canalicular stages. Total RNA was extracted from fetal tissue samples using RNeasy Kit (Qiagen, Germany). First-strand cDNA was synthesized using RevertAid™ H Minus First Strand cDNA Synthesis Kit (Thermo Fisher Scientific, Massachusetts, USA). SYBR® Premix Ex Taq™ II (Tli RNaseH Plus, TaKaRa, Japan) was used for the real time RT-PCR reaction according to the following conditions: denaturation at 94 °C for 30 seconds, annealing at 60°C for 60 seconds, and extension at 72°C for 60 seconds using the Applied Biosystems StepOne (Massachusetts, USA) and analyzed with StepOne software (Version 2.1). The samples were collected from three independent replicates. Comparative CT method ($2^{-\Delta\Delta CT}$) was selected as the method of analysis according to the amplification efficiencies of the housekeeping gene (GAPDH) and target genes primers and the fold changes (compared with ANOVA followed by Bonferroni post hoc as described under the "statistical analysis" below) were shown relative to the control group (human foreskin fibroblast). The sequences of primers are listed in Table 2.

Table 2. Real time RT-PCR primers

| Human primers | Sequence 5'→3' |
|---|---|
| GAPDH | Forward: GACAACAGCCTCAAGATCATCAG |
| | Reverse: ATGGCATGGACTGTGGTCATGAG |
| NKX2 | Forward: GCATGAACATGAGCGGCAT |
| | Reverse: CGACAGGTACTTCTGTTGCTTG |
| SOX2 | Forward: CCCAGCAGACTTCACATGT |
| | Reverse: CCTCCCATTTCCCTCGTTTT |
| MUC16 | Forward: CCAGTCCTACATCTTCGGTTGT |
| | Reverse: AGGGTAGTTCCTAGAGGGAGTT |
| MUC5A | Forward: ATTGCTATTATGCCCTGTGTA |
| | Reverse: TGGTGGACGGACAGTCACT |
| FOXJ1 | Forward: GCATAAGCGCAAACAGCCG |
| | Reverse: TCGAAGATGGCCTCCCAGT |
| SOX9 | Forward: GAGGAAGTCGGTGAAGAACG |
| | Reverse: GTTTTGGGGGTGGTGGGT |
| T1α | Forward: AGAGCAACAACTCAACGGGAA |
| | Reverse: TTCTGCCAGGACCCAGAGC |
| AQP5 | Forward: ACT GGGTTTTCT GGG TAG GG |
| | Reverse: ATG GTCTTCTTC CGCTCT TC |
| SFTPC | Forward: CCTTCTTATCGTGGTGGTGGTGGT |
| | Reverse: TCTCCGTGTGTTTCTGGCTCATGT |
| SFTPA | Forward: TCCAAGCCACACTCCACGA |
| | Reverse: TTCCTCTGGATTCCTTGGG |
| **Rat primers** | |
| GAPDH | Forward: GACCACAGTCCATGACATCACT |
| | Reverse: TCCACCACCCTGTTGCTGTAG |
| IL-10 | Forward: GGCTGCCTTCAGTCAAGTGA |
| | Reverse: GCAACCCAAGTAACCCTTAAAGTC |
| TGF-β | Forward: GTGGCTGTTGCGGAGAGAG |
| | Reverse: ATCTTCGTTGTCCACTCCTTTGA |
| SPC | Forward: TGGACATGAGTAGCAAAGAG |
| | Reverse: GTAGCAGTAGGTTCCTGGAG |
| AQP5 | Forward: CGCTCAGCAACAACACAACACC |
| | Reverse: GACCGACAAGCCAATGGATAAG |

### *Flow cytometry*

The tissues were digested with 1 mg/mL collagenase I/IV (40 minutes), and then centrifuged at 350 g (5 minutes). The cell pellet was re-suspended in PBS. Single cell suspension was achieved using a 70 µm Cell Strainer (Sigma-Aldrich, St. Louis, USA). Propidium iodide (Sigma-Aldrich, St. Louis, USA) cell viability dye (1 µg/mL) was used to exclude dead cells. The cell population with a viability of more than 70% was used. The cells were fixed with 4% (w/v) formaldehyde in PBS (Sigma-Aldrich, St. Louis, USA) at 4 °C (20 minutes), and then washed with PBS. After permeabilization with 0.2% Triton X-100 at room temperature (10 minutes), and blocking in 2% bovine serum albumin (BSA) at 37 °C (15 minutes), the cells were treated with primary antibodies at 4 °C (24 hours) including 1:400, rabbit anti-KRT5; 1:50 mouse anti-KRT14; and 1:200 mouse anti-TRP63 (all from Abcam, Cambridge, USA). The cells were then washed with pre-cooled PBS (4 °C), followed by a 30-minute incubation with secondary antibodies including 1:100, anti-Mouse Alexa Fluor 488, 1:100 anti-Rabbit Alexa Fluor 488 and 1:100 anti-Mouse Alexa Fluor 647 (all from Abcam, Cambridge, USA). Rabbit IgG monoclonal and mouse IgG2a antibodies (both from Abcam, Cambridge, USA) were used as an isotype control. The phenotypic characteristics of the cells were measured by FACSCalibur (Becton Dickinson, USA) (three samples for each test) and analyzed by Flowing Software Version 2.5.1 (Cell Imaging Core, Abo Akademi University, Finland). Data are presented as and histograms.

### *Cell isolation and culture*

Tissues were rinsed three times with PBS supplemented with 100 U/mL penicillin and 0.1 mg/mL streptomycin (Gibco, Gaithersburg, USA), and divided into two parts of tracheobronchial and distal airways/alveolar regions. Each part was cut into pieces of 1×1 mm and treated with 1 mg/mL collagenase I/IV (Gibco, Gaithersburg, USA) in DMEM/F12 at 37 °C (35 min). DMEM/F12 with 10% FBS was added and the samples were centrifuged at 350 g (5 min). The cell pellet was re-suspended in DMEM/F12 supplemented with 10% FBS, 2 mM Glutamax (Gibco, UK), 100 U/mL penicillin/100 µg/mL streptomycin, 10 ng/mL rhEGF (Invitrogen, New York, USA), 10 ng/mL rhFGF10 (R&D Systems, Minneapolis, USA), 10 ng/mL rhKGF (Royan Institute, Iran), 15 mg/mL bovine pituitary extract (Chem Cruz, Texas, USA), and 50 µg/mL retinoic acid (Sigma, Missouri, USA), seeded in dishes coated with 1% (w/v) BSA (Biowest, France), 0.1% (v/v) PureCol (Advanced Biomatrix, Carlsbad, USA), and 0.1% (v/v) fibronectin (Sigma, Missouri, USA), and incubated in a humidified incubator with 5% $CO_2$ at 37 °C. At 80% confluence, the cells were harvested by trypsin/EDTA (Gibco, Gaithersburg, USA), centrifuged at 350 g (5 minutes), and subjected to cell characterizations.

### *Immunostaining of cultured cells*

The isolated cells were cultured and examined on day 4 for the expression of pan-Keratin, KTR5, and Trp63 proteins. The cells were fixed with 4% (w/v) formaldehyde in PBS (Sigma-Aldrich St. Louis, USA) (15 minutes) at room temperature followed by blocking with 10% goat serum at 37 °C (1 hour). After permeabilization with 0.2% Triton X-100 at room temperature (20 minutes), the cells were treated with the primary antibodies diluted in 5% goat serum including 1:100, mouse anti-pan-Keratin (Thermo Fisher Scientific, Waltham, Massachusetts, USA); 1:200, rabbit anti-KRT5 and 1:100, mouse anti-TRP63 (all from Abcam, Cambridge, USA). The samples were washed three times with PBS, followed by 60-minutes incubation

at 37 °C with secondary antibodies including 1:1000, anti-Mouse Alexa Fluor 594; and 1:1000, anti-Rabbit Alexa Fluor 488 (both from Abcam, Cambridge, USA). The samples were washed again with PBS, and nuclei were counterstained for 1 minute with DAPI (Sigma-Aldrich, St. Louis, USA).

### *Organoid formation assay*

Lung organoids were generated for both canalicular and pseudoglandular stages by mixing the cells (passage 0) derived from tracheobronchial and distal airways/alveolar regions with 50% Matrigel (Corning, Life Science, New York, USA) at a density of $2\times10^5$ cells/droplets of 30 µL and gentle pipetting of the cells/Matrigel mixture. Then, droplets were placed in a non-adherent plate and incubated at 37 °C to solidify in 2 hours. Then, DMEM/F12 medium supplemented with 10% FBS and growth factors (10 ng/mL EGF, 10 ng/mL FGF10, 10 ng/mL KGF, 50 µg/mL RA) were added (steroids were not added to the culture medium), droplets were floated by pipetting, and incubated at 37°C in a humidified incubator with 5% $CO_2$ for 10 days. The organoids were not grown on the air-liquid interface.

Before formation of organoids, the percentage of the epithelial cells in the mixed cell population that underwent organoid formation assay, were analyzed by flow cytometry (three samples for each assessment as described above under the title "flow cytometry") using mouse anti-EpCAM-FITC antibody (Miltenyi Biotec, Germany) at day 4 post-culture. As descibed before,[7] organoid samples were collected at days 10 and 21, were fixed with 4% (w/v) formaldehyde in PBS (Sigma-Aldrich, St. Louis, USA) at room temperature for 15 minutes, and underwent histological and real time RT-PCR evaluations as described above under the titles "histological evaluations" and "real time RT-PCR". In real time RT-PCR, the fold changes of target genes in organoid structures were shown relative to the 2D culture-derived cells.

### *Bleomycin-induced rat lung injury and cell therapy*

Male Sprague-Dawley rats (200-230 g) were used for the cell therapy study. Animals were maintained in accordance with guidelines for experimental animals approved by the institutional Committees of Animal Care and Research of Iran University of Medical Science. Lung injury was induced by intratracheal instillation of a single dose of bleomycin (BLM) (2.5 U/kg) (Sigma, Missouri, USA) under Ketamine (90 mg/kg) and Xylazine (10 mg/kg) anesthesia. The animals underwent cell therapy with canalicular stage human fetal lower respiratory tract cells (hFLRTCs) derived from either (a) tracheobronchial or (b) distal airways/alveolar region after flow cytometric evaluation for expression of EpCAM, and epithelial cell marker. After cell therapy, the animals were examined at both early (day 0, 4 hours post-BLM instillation) and late (day 14) phases of the injury.

A minimum of 3 rats were included for each experimental group. Rats were randomly divided into six groups: (1) rats intratracheally instilled with PBS; (2) induced injury with no cell therapy; (3) induced injury followed by tracheobronchial-derived cell therapy at day 0; (4) induced injury followed by tracheobronchial-derived cell therapy at day 14; (5) induced injury followed by distal airways/alveolar region-derived cell therapy at day 0; (6) induced injury followed by distal airways/alveolar region-derived cell therapy at day 14. The cells used for cell therapy were labeled with CM-DiI (5 µL per 1 mL of $10^3$ cells) (Vybrant™ Cell-Labeling, Thermo Fisher Scientific, Massachusetts, USA) in accordance with manufacturer's instructions. The animals received $3\times10^6$ cells (passage 1) intratracheally and euthanized by lethal doses of ketamine and xylazine at day 28.

Histological slides were prepared from the harvested lungs as described under the title "histological evaluations". The slides underwent the antigen retrieval process followed by immersion in a 0.1% $H_2O_2$ solution and blocking with 10% goat serum in PBS at 37 °C (1 hour). Afterwards, the samples were incubated at 4 °C overnight with primary antibodies including rabbit anti-Collagen 1 and rabbit anti-fibronectin (1/100) (all from Abcam, Cambridge, USA) (collagen 1 and fibronectin are the main components of lung extracellular matrix). The day after, samples were incubated for 1 hour at 37 °C with anti-Rabbit-HRP (1:1000) (Abcam, Cambridge, USA) followed by DAB staining. All samples were counterstained with Hematoxylin. Masson trichrome staining was also performed in which the morphological changes in 70 randomly chosen microscopic fields per group were photographed with 20-fold magnification and were quantified according to the numerical scale proposed by Ashcroft et al.[15] Also, RNA extraction has been performed on the harvested whole lungs and real time RT-PCR performed for assessment of expression of inflammatory and fibrotic cytokines and for expression of *SPC* and *AQP5* genes as described above under the title "real time RT-PCR". The sequences of primers are listed in Table 2.

### *Statistical analysis*

Statistical analysis was performed using GraphPad Prism (Version 6.1, GraphPad software, CA, USA). The normality of distribution of data and equality of variances were tested by Kolmogorov-Smirnov and F tests respectively in order to determine the method of comparison (parametric or non-parametric). Parametric comparison of means was performed by t-test and ANOVA (with Bonferroni post-hoc), where appropriate; and comparison of proportions was performed by $\chi^2$ test. Statistical significance of differences between two groups of data were determined by multiple t-test. Data are presented as mean ± standard deviation (SD). Mean differences were considered statistically significant at $P<0.05$.

## Results

### *Distribution of basal cell subpopulations in human fetal tracheobronchial epithelium*

H&E staining showed that both trachea and bronchi were populated with stratified epithelium in both pseudoglandular and canalicular stages (Fig. 1B-I). Epithelial cells and stem cells were identified by expression of pan-Keratin and co-expression of KRT5. These cells were mostly localized in the basal layer of both trachea and bronchi in both stages (Figs. 1B-II and IB-III and Figs. 2A-I, 2B-I). Also, our results revealed that KRT5$^{+}$/KRT14$^{+}$ cells populated these regions in both stages (Figs. 2A-II and 2B-II). In contrast to the KRT5$^{+}$ cells, which distinctly covered the basal layer, TRP63 was widely expressed and distributed from the basal to the superficial layer of the epithelium. In addition, co-staining revealed the presence of the KRT5$^{+}$/TRP63$^{+}$ population that was limited to the basal layer of the epithelium of trachea and bronchi in both stages (Figs. 1B-II and IB-III and Figs. 2A-III, 2B-III).

### *Quantification of basal cell subpopulations in human fetal tracheobronchial epithelium*

Immunostaining data revealed that KRT5 and KRT14 were expressed in the trachea of both stages without significant differences (Fig. 2C). At the same time, TRP63$^{+}$ cells decreased in the trachea of the canalicular stage (49±4%) (*P<0.05*) compared to pseudoglandular stage (82±4%). Similar to the trachea, TRP63$^{+}$ cells decreased in the bronchi of the canalicular stage (*P<0.05*), whereas KRT5 expression increased in the bronchi of the canalicular (89±6%) compared to pseudoglandular stage (45±6%) (*P<0.01*) (Fig. 2D). The same examination in the bronchi of both stages revealed a decrease in TRP63 expressing cells (61±11%, *P<0.05*) and an increase in

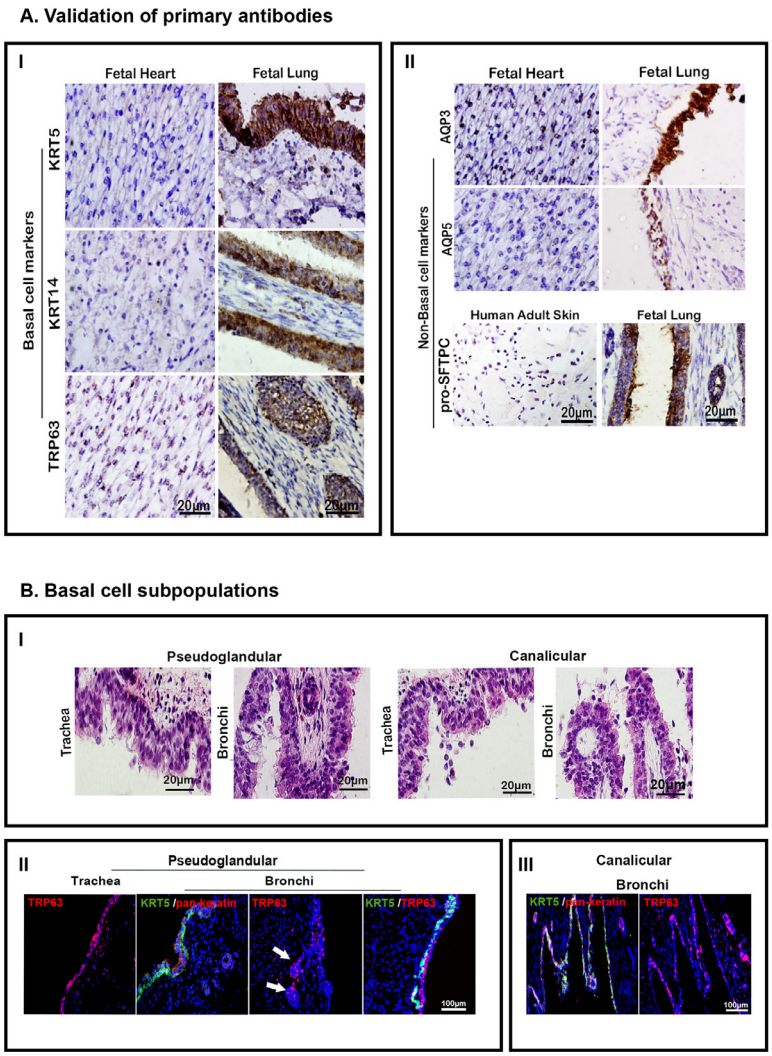


**Fig. 1. Antibodies' validation and basal cell subpopulations.** (A) Validation of primary antibodies for immunohistochemical applications by positive and negative samples confirming their validity. (I) representation of basal epithelial cell markers in fetal heart (left column) and fetal trachea of canalicular stage (right column). (II) Representation of lineage restricted or non-basal cell markers in fetal heart and human adult skin (left column) and trachea (right column). Scale bar = 20 µm (for all photomicrographs). (B) Staining for basal cell subpopulations in human fetal tracheal and bronchial epithelium showing their distribution. (I) H&E staining showing pseudostratified epithelium. (II-III) immunohistochemical staining: pan-Keratin is the marker of epithelial cells; white arrows show TRP63+ cells in developing sub-mucosal glands; Scale bar = 100 µm (for all fluorescent photomicrographs).

KRT5$^+$ cells (85±6%, *P<0.01*) throughout the transition from pseudoglandular to the canalicular stage (Fig. 2D). Scoring of double immunostaining (Figs 2C-D) results showed that an extensive area of the tracheal epithelium was populated with KRT5$^+$/KRT14$^+$ (58.33% in pseudoglandular and 63.44% in canalicular) and KRT5$^+$/TRP63$^+$ (58.33% in pseudoglandular and 50.34% in canalicular). Besides these populations, the tracheal epithelium of pseudoglandular and canalicular stages was covered with other cell populations, including KRT5$^-$/KRT14$^+$, KRT5$^-$/KRT14$^-$, KRT5$^-$/TRP63$^+$, and KRT5$^-$/TRP63$^-$. In the canalicular stage, KRT5$^-$/TRP63$^-$ was the major population (36.57%) after KRT5$^+$/KRT14$^+$ and KRT5$^+$/TRP63$^+$ (Fig. 2C).

### *Distribution and quantification of basal cell subpopulations in human fetal DA/AR*

Some of the distal airways showed KRT5$^+$ cells in the basal layer, while the superficial layer epithelium in distal airways and all developing alveoli were negative for KRT5 phenotype in both stages (Fig. 3A). In addition, co-localization of KRT5 and KRT14 markers was observed only in distal airways (Fig. 3B). Expression of TRP63 was extensively detected in all distal airways and developing alveoli in both stages (Fig. 3C). As shown in Fig. 3D, more than 90% of epithelial cells in distal airways and alveolar

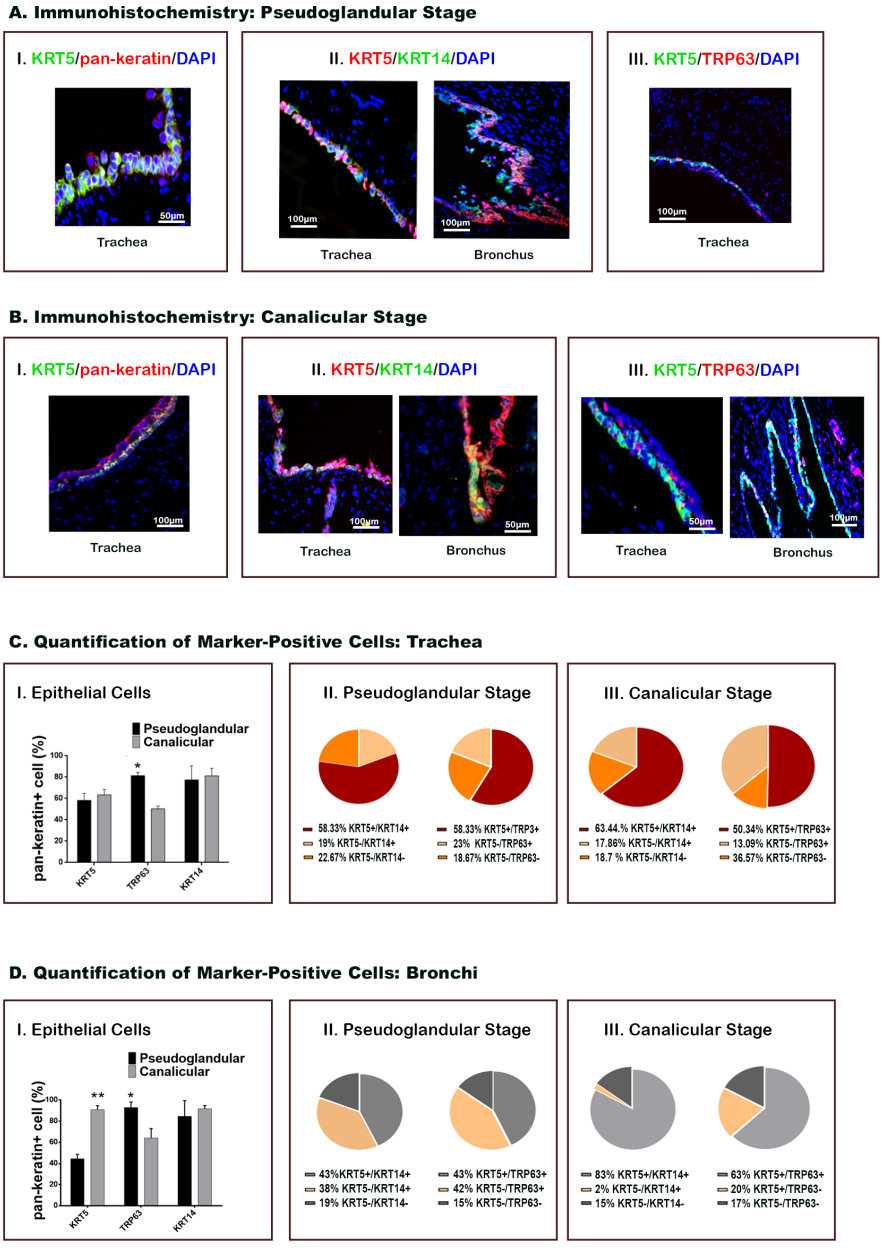


**Fig. 2. Basal cell markers in proximal airways,** showing distribution and quantification of positive cells. (A-B) Immunohistochemical staining shows epithelial cells during pseudoglandular and canalicular stages in both tracheal and bronchial tissues. Each marker is labeled by the color represented in the photomicrograph. (C-D) Quantification of the cells positive for specific molecular markers is presented for both trachea and bronchi (*$P$ < 0.05, **$P$ < 0.01; n = 24, $\chi^2$ test).

region in pseudoglandular and 70% in canalicular stages were TRP63$^{+}$. However, the percentages of KRT5$^{+}$ and KRT14$^{+}$ cells did not show significant differences between pseudoglandular and canalicular stages.

Corresponding to immunostaining findings, most distal airway epithelial cells (63.70% in pseudoglandular and 41.70% in canalicular) were KRT5$^{-}$/KRT14$^{-}$ and distributed in the superficial layer of the epithelium. However, 9.7% of epithelial cells in the distal airways of pseudoglandular stage revealed a KRT5$^{+}$/KRT14$^{+}$ phenotype, and this population increased up to 21.4% in the canalicular stage (Fig. 3E).

### *Expression of non-basal cell markers in human fetal tracheobronchial and distal airways epithelium*

Extensive positive areas for AQP3 and pro-SFTPC were identified in the tracheobronchial epithelium in both stages. The immunostaining result revealed the distribution of AQP3$^{+}$ and pro-SFTPC$^{+}$ cells from the basal layer to the superficial layer in the stratified epithelium of both trachea and bronchi and submucosal glands (Figs. 4A-B). The relative expression of molecular marker genes of early progenitor cells in the tracheobronchial region of both stages (Fig. 4C) showed that *SOX2* and *SOX9* were upregulated throughout the transition from

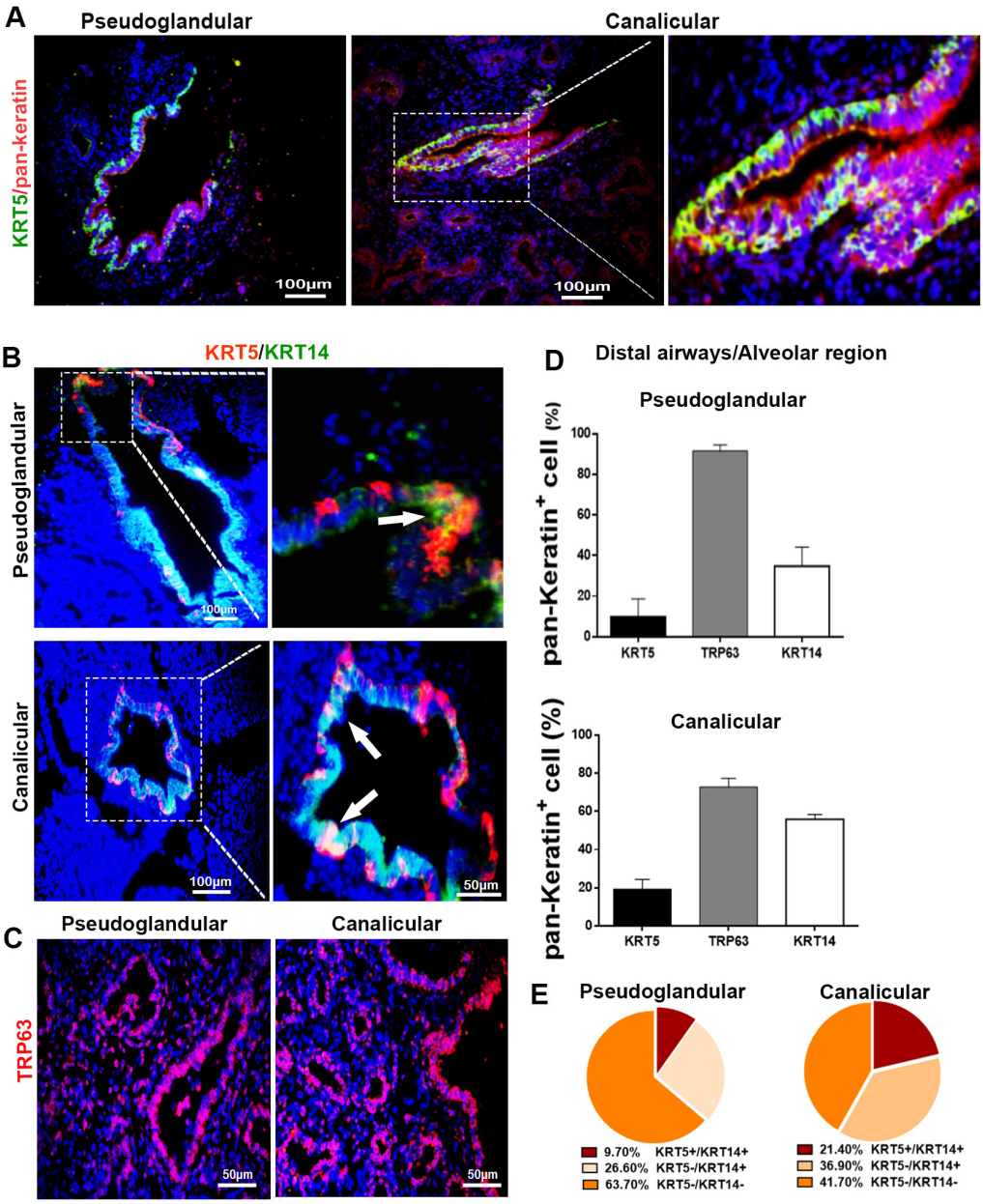


**Fig. 3. Basal cell markers in distal airways/alveolar regions,** showing distribution and quantification of positive cells. (A-C) immunohistochemical staining showing epithelial cells during pseudoglandular and canalicular stages. Each marker is labeled by the color represented in the photomicrograph; white arrows show the co-localization of KRT5 and KRT14. (D-E) Quantifying the cells positive for specific molecular markers (n = 24).

pseudoglandular to canalicular. At the same time, *NKX2.1* was decreased in the canalicular stage.

The results revealed the distribution of AQP3⁺ cells only in distal airways, not in developing alveolar structures of both stages (Fig. 4D). Distal airways of pseudoglandular stage showed the expression of pro-SFTPC in both basal and superficial epithelial layers. In contrast, in the canalicular stage, expression of pro-SFTPC was observed only in the superficial layer of the epithelium (Fig. 4E). Additionally, pro-SFTPC was detected in the alveolar region in both stages. TEM micrographs showed developing lamellar bodies only in the alveolar region in the canalicular stage from 19pcw (post-conception weeks) (Fig. 4F-H) along with glycogen vesicles (GVs). Lamellar bodies and GVs were not detected in the pseudoglandular stage.

Expression analysis of molecular marker genes of early progenitor cells showed significant decreases in *NKX2.1* from pseudoglandular to canalicular stages (Fig. 4I), whereas *SOX9* significantly increased in the canalicular stage in DA/AR.

### *Evaluation of isolated primary epithelial cells*

The viabilities of cells isolated from pseudoglandular and canalicular stages were 88.21% and 80.54%, respectively (Fig. 5A). The percentages of the cells expressing KRT5, KRT14, and TRP63 were determined by flow cytometry (Fig. 5B), showing that KRT5⁺ cells decrease from proximal to distal airways in both pseudoglandular ($P$<0.001) and canalicular ($P$<0.001) stages. The same proximal-distal pattern of decreasing expression was also observed for KRT14⁺ cells in the pseudoglandular stage ($P$<0.05). Analysis of the percentage of marker-positive cells in the pseudoglandular-canalicular axis showed that TRP63⁺ cells decrease in DA/AR from pseudoglandular to canalicular stage ($P$<0.001). The highest expression level of TRP63 was observed in DA/AR of pseudoglandular stage (74.97±9%) (Fig. 5B).

### *A minor subset of tracheobronchial cells give rise to distinct colonies in 2D culture*

On day 4 of culture, the cells were characterized for expressing pan-Keratin, KRT5, and Trp63. The cells

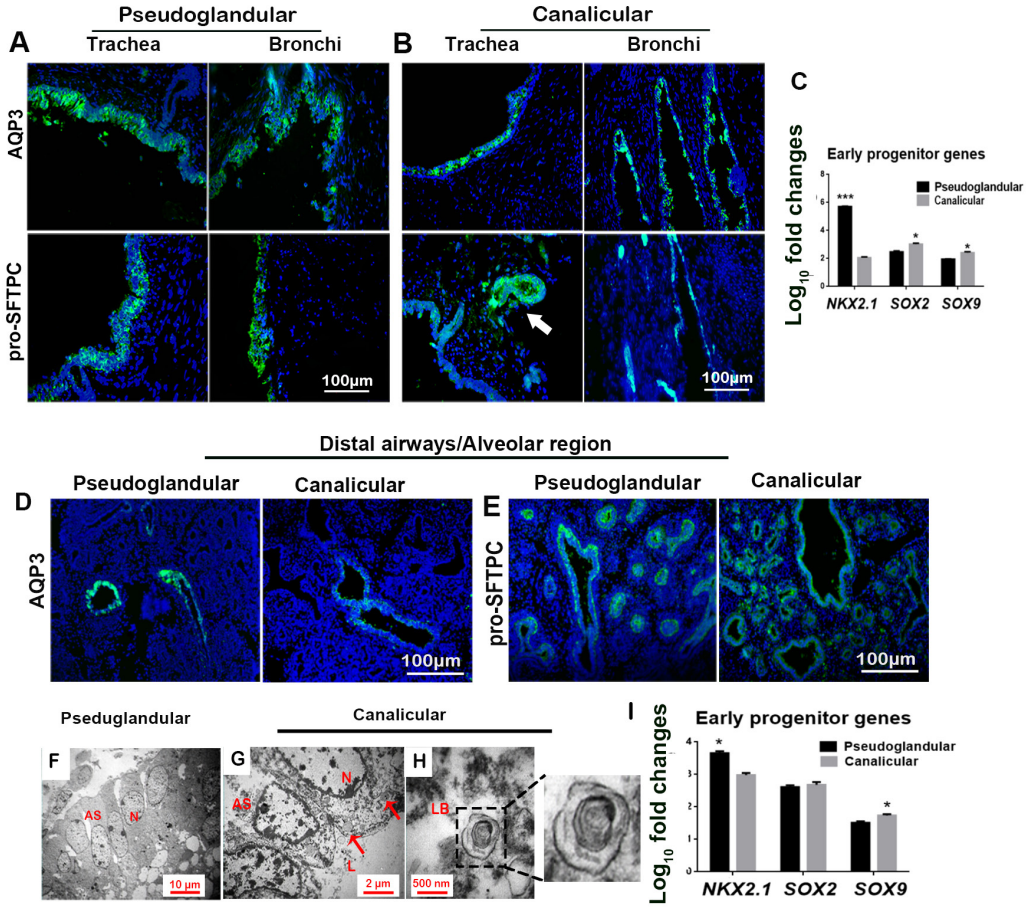


**Fig. 4. Non-basal cell markers in proximal and distal airways/alveolar regions,** showing distribution and quantification of positive cells. (A-B) immunohistochemical staining: white arrow shows pro-SFTPC⁺ cells in developing sub-mucosal glands. (C) Gene expression levels in tracheobronchial epithelium (*$P$ < 0.05 and ***$P$ < 0.001; n = 3, t-test). (D-E) immunohistochemical staining; (E) Expression of pro-SFTPC by basal cells in higher magnification (white arrows). (F-H) TEM of epithelial cells showing developing alveolar structures (AS) with large nuclei (N), glycogen vesicles (red arrows); lumen (L). and a lamellar body (LB; with a magnified inset [×2]); (I) Gene expression levels in distal airways/alveolar region epithelium (*$P$ < 0.05 and ***$P$ < 0.001; n = 3, t-test).

isolated from tracheobronchial and DA/ARs exhibited typical epithelial colony morphology (Figs. 5C-F). The epithelial cells in the isolated cell population were identified by immunostaining for pan-Keratin expression (Figs. 5G-J). A subset of epithelial cells expressed KRT5 and TRP63 markers in the tracheobronchial region of both stages with different features of colonies. In the pseudoglandular stage, tracheobronchial-derived epithelial cells formed distinctive KRT5$^+$ (including KRT5$^+$/TRP63$^+$) colonies with well-defined borders (Figs. 5K and 5O). In contrast, epithelial cells in DA/AR and the canalicular stage did not form any distinctly defined KRT5$^+$ colony; only a few KRT5$^+$ cells could be detected in DA/AR and in the canalicular stage (Figs. 5L-N and 5P-R), which conforms to the flow cytometric findings.

### *Organoid assay*

The flow cytometry analysis of the cells that underwent organoid assay showed that out of those isolated in the canalicular stage, 46.3% of tracheobronchial cells and 32% of airways/alveolar cells were EpCAM$^+$ (Figs. 6A-B). H&E staining of organoids revealed that the epithelial cells formed a self-organized structure in 3D culture. Tracheobronchial-derived cells formed a structure with a small lumen covered with a multi-layer epithelium (Figs. 6C-D). DA/AR-derived organoids of the canalicular stage

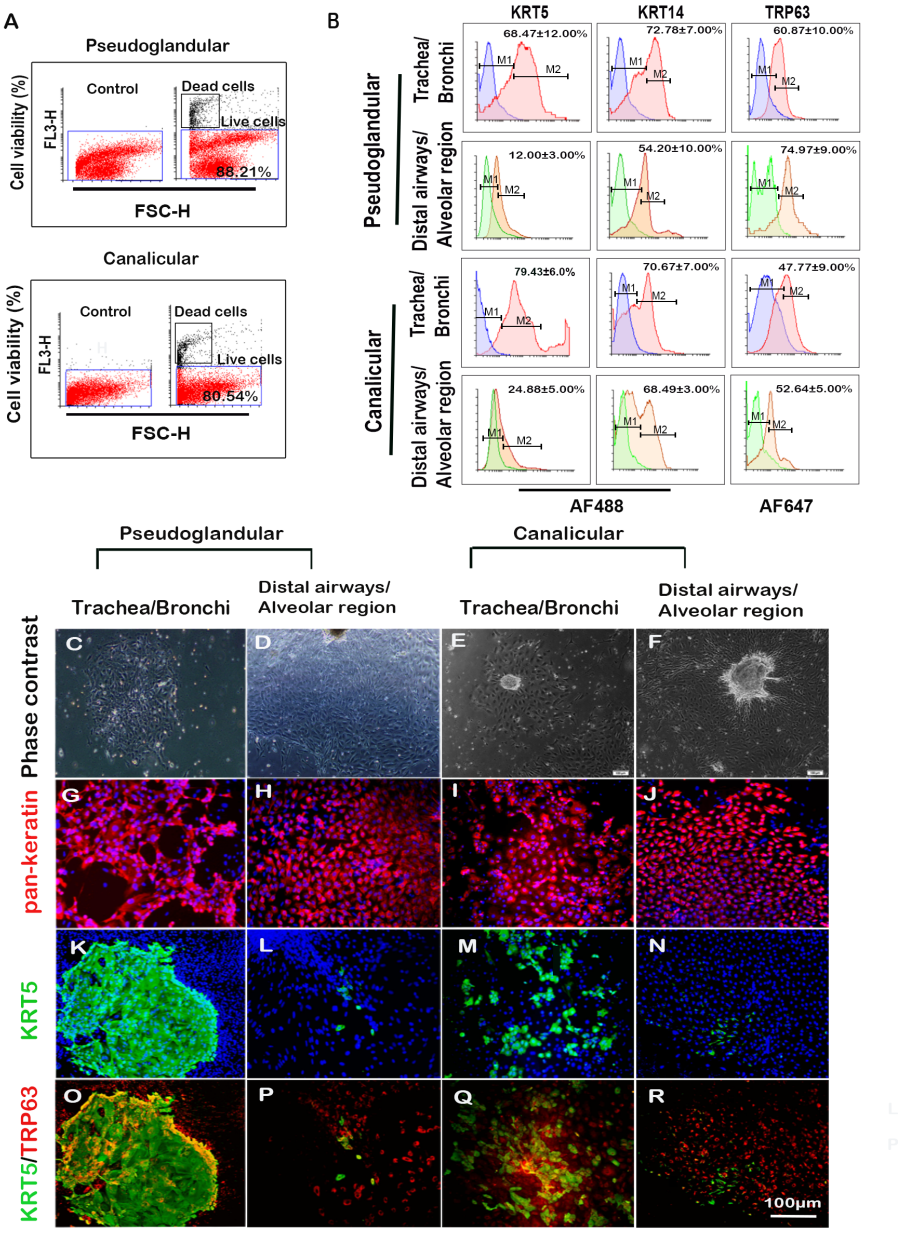


**Fig. 5. Characterization of isolated cells,** showing their molecular markers expression profile. (A) Flow cytometry for cell viability using PI staining and (B) expression of basal cell markers; blue and green histograms are from isotype control; red and orange histograms are from test groups (n = 3, mean±SD). (C-F) typical epithelial colonies. (G-R) immunocytochemical staining showing distinct basal cell colonies (K and O). Scale bar equals 100 µm (for all fluorescent photomicrographs); AF488 Alexa Fluor 488, AF647 Alexa Fluor 647.

formed a structure with a large lumen covered with a monolayer epithelium (Fig. 6E).

Flow cytometry of the cells from organoids of pseudoglandular stage showed that 28% of distal airways/alveolar cells were EpCAM+ (Fig 6J). H&E staining of 10- and 21-day organoids derived from DA/AR of pseudoglandular stage showed that the structures formed in these organoids comprise a columnar epithelial cell organization and alveolar-like structures (Figs. 6K and M).

The presence of pan-Keratin$^+$ cells showed the contribution of epithelial cells in the lumen of the structures formed in organoids (Figs. 6F-G). The other findings were co-expression of KRT5/TRP63 in these epithelial cells, which indicates the contribution of progenitor cells (Figs. 6H-I), and expression of AQP-5 in 10-day organoids (Fig. 6L) and pro-SFTPC in 21-day organoids (Fig. 6N), which indicate alveolar differentiation. We could not detect the expression of AQP-5 in 21-day organoids and pro-SFTPC in 10-day organoids. Continuous expression of TRP63 was observed after 21 days in organoids of pseudoglandular stage. But, expression of epithelial stem cell marker (KRT5) was not detected in 21-day organoids (Fig. 6N).

The expression levels of early progenitor molecular marker genes, ciliated, secretory, AEC1, and AEC2/club cells isolated from distal airway/alveolar region and cultured in 3D conditions (organoids) were compared with those cultured in 2D conditions for 21 days (Fig. 6O). The results revealed that the mRNA expression levels of early lung progenitor genes were higher in organoids. However, KRT5 protein could not be detected in 21-day organoids (Fig. 6N). Increased expressions of all other genes compared to 2D culture conditions were also detected.

### *Cell therapy with hFLRTCs for a rat pulmonary injury model*

Our results revealed that 35% and 53% of the mixed

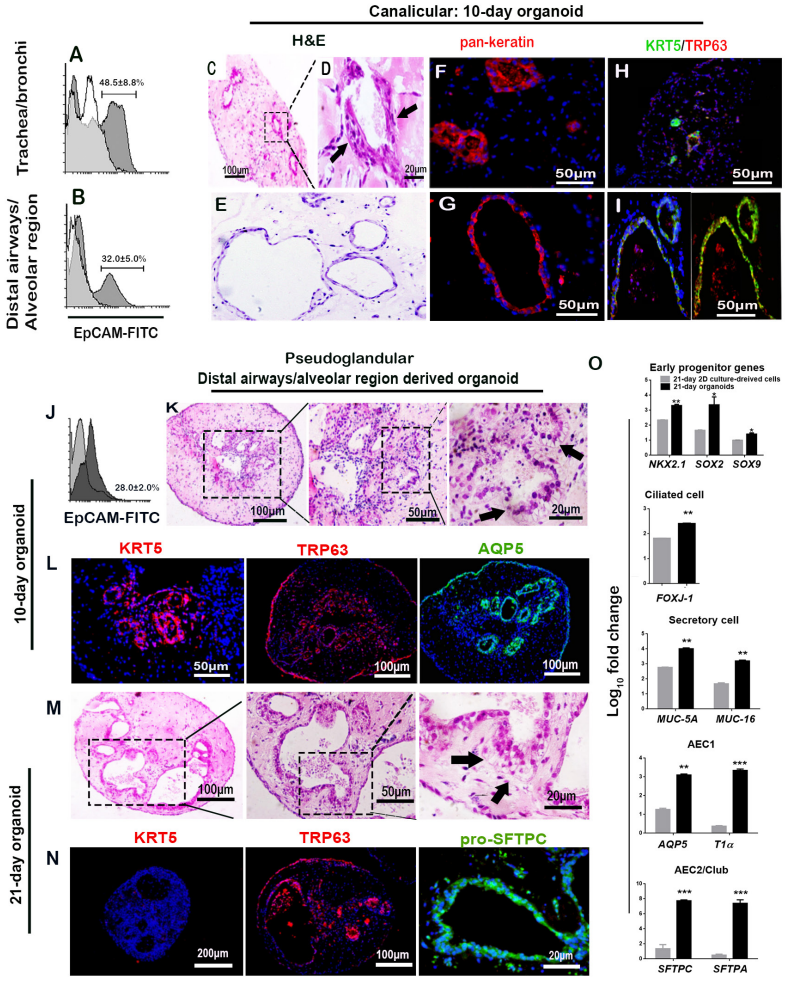


**Fig. 6. Organoid culture,** showing the contribution of spatial niche for modulation of potency of respiratory progenitor cells. (A-I) Canalicular stage including: (A-B) Flow cytometry for EpCAM$^+$ cells that underwent organoid assay (n = 3, mean±SD); (C-E) H&E staining showing self-assembled structures (black arrows); (F-I) Contribution of pan-Keratin$^+$ and KRT5$^+$/TRP63$^+$ cells to organoid structures. (J-N) Pseudoglandular stage including (J) Flow cytometry for EpCAM$^+$ cells that underwent organoid assay (n = 3, mean±SD); (K) H&E staining showing columnar epithelial cells (black arrows) and (L) immunostaining for basal cells (KRT5 and TRP63) and non-basal cells (AQP-5) in 10-day organoids; (M) H&E staining showing columnar epithelial cells (black arrows) and (N) immunostaining in 21-day organoids. (O) Gene expression levels of molecular marker genes in organoids relative to the cells cultured in 2D conditions for 21-days (*$P$ < 0.05, **$P$ < 0.01, and ***$P$ < 0.001; n = 3, t-test).

cell populations derived from the trachea and DA/AR expressed EpCAM, respectively (Fig. 7A). The EpCAM-negative cells were fibroblast-like cells expressing vimentin (data not shown). As shown in Fig. 7B, in the animals that received BLM but did not undergo cell therapy (+BLM/-Cell), the lungs had macroscopic fibrotic features, including a large and pale appearance with several scars as compared with the lungs of the animals that did not receive BLM (-BLM/-Cell). BLM instillation was associated with fibrosis and collagen deposition leading to a marked increase in lung weight ($P$<0.01). However, cell therapy could significantly prevent weight gain in the affected lungs ($P$<0.05) (Fig. 7C).

Masson trichrome staining showed that cell therapy modulated the development of fibrosis and led to lower collagen deposition (Fig. 7D). Using immunostaining, we demonstrated an extensive expression of collagen I and fibronectin (as the main components of lung extracellular matrix) in the parenchyma of BLM-treated lungs accompanied by abnormal alveolar architectures. We also showed that cell therapy prevented the upregulation of collagen I and fibronectin expression and substantially improved the alveolar structures. However, it could not return the pattern of collagen I and fibronectin expression and the architecture of alveoli back to a completely normal phenotype (Fig. 7D). The median Ashcroft score for histological sections from animals that did not receive BLM and cell therapy was 1, while that for bleomycin-treated lungs that did not receive cell therapy was 4 ($P$<0.01). In contrast, the progress of fibrosis in animals that received hFLRTCs after BLM instillation on days 0 and 14 was significantly diminished with the median Ashcroft scores of 2 and 3, respectively ($P$<0.05) (Fig. 7E).

To assess the effects of hFLRTCs transplantation, we

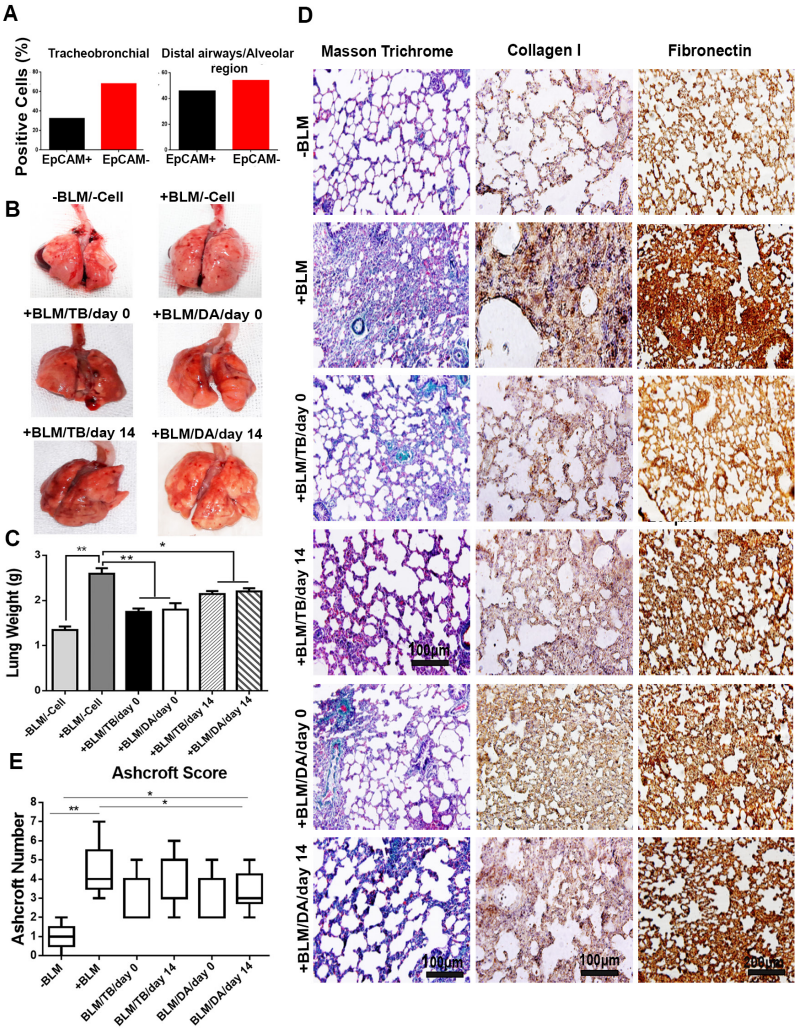


**Fig. 7. Intratracheal administration of cells following bleomycin-induced lung injury,** showing amilioration of lung injury. (**A**) Results of flow cytometric analysis of the mixed cell population for EpCAM expression before transplantation (n = 6). (B) Representative images of whole lungs from all the experimental groups after harvest on day 28 (3 rats for each group). (**C**) Comparison of lung weights after cell therapy (two lobes from the right and left lung/rat, 3 rats; ANOVA followed by Bonferroni posthoc). (**D**) Masson trichrome and immunohistochemical staining showing low interstitial collagen deposition in all the rats underwent cell therapy; (**E**) Ashcroft scoring of histological sections. Distributions are presented as box plots with lines at the lower quartile, median and upper quartile. Whiskers are representative of the minimum and maximum, excluding outliers. -BLM: not-treated with BLM; -Cell: not-underwent cell therapy; +BLM: treated with BLM; /TB: underwent cell therapy with tracheobronchial-derived cells; /DA: underwent cell therapy with distal airways/alveolar region-derived cells; /day 0: underwent cell therapy at day 0; /day 14: underwent cell therapy at day 14; * $P$ < 0.05; and ** $P$ < 0.01

determined the expression of inflammatory and fibrotic cytokines in lung tissue by real-time RT-PCR on day 28 (Fig. 8A). Except for the group treated with DA/AR-derived cells on day 14, other experimental groups showed upregulation of the expression of *IL-10* ($P<0.001$) (up to 17.22 folds in the group that underwent cell therapy with distal airways/alveolar region-derived cells on day 0). Interestingly, *TGF-β*, one of the main fibrosis markers, was down-regulated in all experimental groups ($P<0.01$ and $P<0.001$) (up to 5.89 folds in the group that underwent cell therapy with distal airways/alveolar region-derived cells on day 14).

Analysis of gene expression demonstrated that all the animals that underwent cell therapy exhibited a significant up-regulation in *SPC* compared to those BLM-treated animals that had not received any cells (Fig. 8B). Also, those who received cells at day 0 showed a higher gene expression level (2.71 folds) than day 14 recipients. Moreover, cell therapy decreased *AQP5* expression compared to the BLM-treated animals that had not received any cells ($P<0.001$), and also, a higher down-regulation of *AQP5* (3.28 folds) has observed in day 0 cell therapy groups as compared to the day 14th ($P<0.05$). On the other hand, immunohistochemical staining of the alveolar region (Fig. 8C) showed rarely engrafted DiI-positive tracheobronchial-derived cells transplanted at day 0 expressing AQP3.

## Discussion

This study re-examines the distribution and phenotype of epithelial cells in the human fetal lower respiratory tract during pseudoglandular and canalicular stages. It also examines the role of the "spatial niche" on modulation of the potency of respiratory progenitor cells using an organoid assay and shows that human fetal respiratory cells are potential sources for cell therapy after lung injury.

We show that in fetal trachea and bronchi, basal cells (as stem cells), with KRT5$^+$/KRT14$^+$ and KRT5$^+$/TRP63$^+$ phenotypes, populate the epithelium, particularly at the basal layer, and have a distribution similar to adult bronchi. However, in contrast to adults, in whom 40% of KRT5$^+$ cells co-express the KRT14 and all TRP63$^+$ cells co-express KRT5,[16] we report that in fetal bronchi, all of the KRT5$^+$ cells express KRT14. We also report that only 51% of TRP63+ cells co-express KRT5 in pseudoglandular stage. This ratio increases to 100% in the canalicular stage. Our other interesting finding is that 100% of the KRT5$^+$ cells in the tracheal epithelium are TRP63$^+$ and KRT14$^+$,

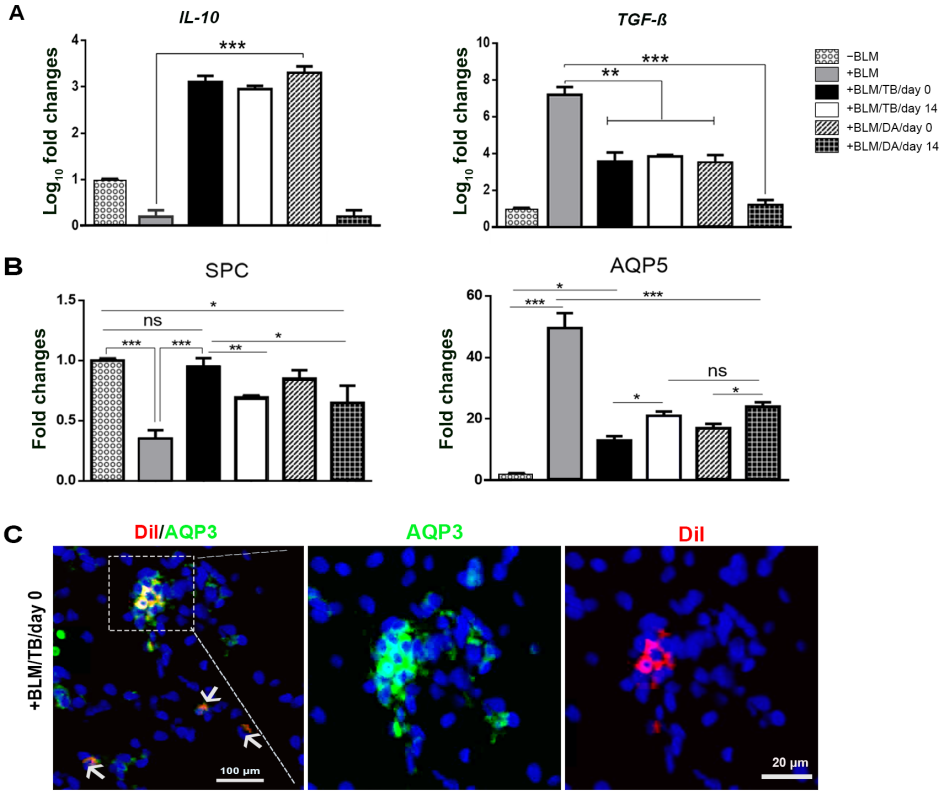


**Fig. 8. Analysis of gene expression following cell therapy,** showing the post-therapy profiles of cytokines. Whole lung RNA extract real-time RT-PCR analysis of expression levels of (**A**) inflammatory-related and fibrotic-related genes and (**B**) *SPC* and *AQP5* genes. **(C)** representative image of the alveolar section showing AQP3 expression by the engrafted hFLRTCsDiI-labeled cells. -BLM: not-treated with BLM; -Cell: not-underwent cell therapy; +BLM: treated with BLM; /TB: underwent cell therapy with tracheobronchial-derived cells; /DA: underwent cell therapy with distal airways/alveolar region-derived cells; /day 0: underwent cell therapy at day 0; /day 14: underwent cell therapy at day 14; (n = 3, * $P < 0.05$; ** $P < 0.01$; *** $P< 0.001$; ANOVA followed by Bonferroni post hoc)

which is not the case in adults.[17] Also, we show a distinct distribution of KRT5$^+$ cells in the basal layer and TRP63$^+$ cells in both basal and superficial layers of the fetal epithelium. This does not conform to the distribution of these cells in the adults, which is reported to be TRP63$^+$ cells in the basal layer and KRT5$^+$ cells in both basal and superficial layers.[16]

In fetal DA/AR, we identify KRT14$^+$ cells, which have not been identified in adult distal airways.[16] Also, we show a proximal to distal decrease in KRT5$^+$ and an increase in TPR63$^+$ cells in the fetal period, which is maintained during adulthood for KRT5$^+$ cells but is reversed for TPR63$^+$ cells.[16]

Our other finding on colony formation potential shows that KRT5$^+$/TRP63$^+$ cells isolated in the pseudoglandular stage from tracheobronchial epithelium have a higher potential to form distinct colonies compared to the other cells in this study. This could be attributed to a higher competence of these cells in a hierarchical differentiation model.

We show that the distribution of AQP3$^+$ cells in the fetal tracheobronchial epithelium is similar to adults[18] and report that the tracheobronchial AQP3$^+$ cells do not show presumed structural characteristics of alveolar types I cells, which conforms to previous reports.[3,19] In fetal distal airways, we interestingly demonstrate an extensive presence of AQP3$^+$ cells in both basal and superficial layers of the epithelium of pseudoglandular, which conforms to bronchiolar distribution in adults, and only in the superficial layer of epithelium in the canalicular stage. We could not identify any AQP3$^+$ cells in the alveolar region in these stages. On the other hand, our findings on the distribution of pro-SFTPC$^+$ cells agree with previous reports.[20,21] However, developing lamellar bodies could not be detected by ultrastructural studies earlier than 19pcw.

The tracheobronchial expressions of SOX2 and SOX9 have not been fully explored during human fetal development. We show that the total expression of SOX2 and SOX9 in the tracheobronchial region increases in canalicular compared with the pseudoglandular stage. On the other hand, human fetal distal tip epithelial cells co-express both SOX2 and SOX9 in pseudoglandular, but express only SOX9 in the canalicular stage. Also, the epithelium of terminal and respiratory bronchioles only expresses SOX2 during both stages.[3, 5] Here, we report the expression levels of these genes in DA/AR and show that expression of SOX9 increases in the canalicular stage. This could result from increased expression of SOX9 in the distal tip epithelium. Our other finding is a stable expression of SOX2 in both stages, which shows that the same level of expression of this gene is needed in the distal lung during both stages.

NKX2.1 is one of the key genes regulating lung development and its postnatal stem cells' function. Our findings on the expression of this gene in proximal airways of the human fetus are consistent with previous reports.[22,23] However, we showed a mild but significant decrease in expression of this gene in the distal lung during canalicular as compared with pseudoglandular stage. This finding results from a precise real-time RT-PCR quantification, which might seem slightly different from a previous report showing the same level of expression of this gene in both stages.[22] However, it should be considered that the latter report is the result of a semi-quantitative immunohistochemical analysis.

The contribution of cellular and extracellular components in the formation of tissue-specific niches and the effects of their manipulations has long been appreciated in the lungs.[24,25] Here, we show that the "spatial niche" should also be taken into account. Our organoid formation assay findings emphasize this spatial niche's critical role in modulation of the progenitor cells' potency in developing respiratory system. Our observation agrees with previous studies reporting the formation of pulmonary organoids from mixed cells of murine fetal lung[26] and human pluripotent stem cells.[27] It should be noted that our observations are based on qualitative examinations. So, it remains to be determined whether cells from one region or developmental stage perform differently and whether a single cell, alone, can develop into the resulting structures.

Our in vivo experiment shows that the cells derived from the fetal lower respiratory tract can ameliorate the lung injury by modulation of expression of fibronectin and collagen I, collagen deposition, Ashcroft score, restoration of lung alveolar structures, and a decrease in lung weight gain after injury. We have shown that the earlier the cell therapy is delivered, the better the regenerative response. It should be noted that in this study, we have established and treated an acute lung injury model. To extend the results of the current report to IPF, a separate study should be performed, which should consider that most patients with IPF are diagnosed at later stages of the disease.

Several reports show a fibrogenic role for TGF-β[28] and an anti-fibrogenic role for IL-10 through suppression of TGF-β[28-30] after lung injury. We have observed a down-regulation of TGF-β expression in all the animals that received cell therapy and an upregulation of the IL-10 in all the animals except those that received distal airways/alveolar-derived cells at day 14.

We have detected very few human fetal cells engraftment in the regenerating host tissue of our immunocompetent rat model (Fig. 8C). Accordingly, it could be hypothesized that paracrine effects resulting from secreted mediators could be considered the dominant mechanism that mediated the injury repair in this experiment. Future studies, such as evaluating cytokine antagonists that can disrupt fibrosis signaling pathways and human lung fetal cell-secreted chemokine screening for fibroblast proliferation-inhibiting factors or factors promoting collagen degradation are needed to elucidate the underlying mechanisms by which hFLRTCs promote the

## Research Highlights

**What is the current knowledge?**

√ Cell therapy with fetal respiratory cells from sources other than humans can ameliorate lung injury in animal models

√ The major phenotypic details of human fetal lower respiratory cells are available from the studies that are not up-to-date

**What is new here?**

√ We provide substantial evidence that human fetal respiratory tract cells can improve the regenerative process after lung injury

√ Our extensive characterization provides an updated phenotypic profile of human fetal lower respiratory cells from 12–19 weeks of gestation

recovery of injured respiratory tissues.

Our other findings are the patterns of expressing specific markers of alveolar types I and II cells in regenerating lungs. According to previous reports, BLM induces aberrant deposition of ECM and disruption of the epithelial basement membrane, which results in irregular differentiation of ATII cells to ATI cells.[31] This is demonstrated by lower expression of SPC and higher expression of AQP5 in our injury model. Our finding of increased expression of SPC and decreased expression of AQP5 after cell therapy shows that our fetal cells improve the gene expression pattern after lung injury to orchestrate the regeneration process.

It should be noted that although the clinical application of fetal cell therapy is a subject of a major controversy due to the source of the cells, the lessons learned by studying legally aborted fetal tissues can improve our understanding of the mechanisms that govern the process of injury repair and can help the development of novel treatment modalities.

## Conclusion

In conclusion, we have shown that fully characterized fetal human lower respiratory tract cells have a high potential to restore the structure and pattern of gene expression in a standard experimental model of lung injury. This is proof of the concept that tissue-derived fetal cells can restore the same adult tissue's injury. Their phenotype could be set as a target when reparative cells are to be obtained from the differentiation of other stem cells, including pluripotent cells.

### Acknowledgments

The authors would like to thank Mahshad Dorraj and Payam Taheri for their contribution to immunostaining troubleshooting, imaging, and image analysis; and Pardis Khosravani and Masoomeh Azimi for their flow cytometry technical support.

### Authors Contribution

**Conceptualization:** Fatemeh Ganji, Hamid Reza Aghayan, Ali Samadikuchaksaraei.
**Data curation:** Fatemeh Ganji.
**Formal analysis:** Fatemeh Ganji, Nushin Karkuki Osguei, Ali Samadikuchaksaraei.
**Funding acquisition:** Ali Samadikuchaksaraei.
**Investigation:** Fatemeh Ganji, Ali Shirani, Mahtab Golmohammadi.
**Methodology:** Fatemeh Ganji, Ali Samadikuchaksaraei.
**Project administration:** Hamid Reza Aghayan.
**Resources:** Marzieh Ebrahimi, Maryam Kashanian, Kiana Koolaeinezhad, Hamid Reza Davari, Seyed Ali Javad Mousavi, Hamid Reza Aghayan, Babak Arjmand, Ramin Heshmat, Ali Samadikuchaksaraei.
**Supervision:** Ali Samadikuchaksaraei.
**Validation:** Ali Samadikuchaksaraei.
**Visualization:** Fatemeh Ganji.
**Writing–original draft:** Fatemeh Ganji, Ali Samadikuchaksaraei.
**Writing–review editing:** Fatemeh Ganji, Marzieh Ebrahimi, Ali Shirani, Mahtab Golmohammadi, Mazaher Gholipourmalekabadi, Maryam Kashanian, Kiana Koolaeinezhad, Hamid Reza Davari, Seyed Ali Javad Mousavi, Hamid Reza Aghayan, Babak Arjmand, Ramin Heshmat, Nushin Karkuki Osguei, Ali Samadikuchaksaraei.

### Competing Interests

The authors declare no competing interests.

### Ethical Statement

This study was carried out according to the Code of Ethics of the World Medical Association (Declaration of Helsinki) under the approval of the Ethical Committees of the Iranian Ministry of Health (code: EC-00264, 17 August 2013) and the Iran University of Medical Sciences (IUMS) (code: IR.IUMS.rec.1393.25093, 30 September 2014). All fetal and adult tissues were obtained with written informed consent.

### Funding

This work was supported by grants from the Iran University of Medical Science (93-03-87-25093, 95-03-159-29402) and the Iranian Council for Development of Stem Cell Sciences and Technologies (11/79319).

### References

1. Hosseinirad H, Rashidi M, Moghaddam MM, Tebyanian H, Nouraei S, Mirhosseini SA, *et al.* Stem cell therapy for lung diseases: From fundamental aspects to clinical applications. *Cell Mol Biol (Noisy-le-grand)* **2018**; 64: 92-101.
2. Rosen C, Shezen E, Aronovich A, Klionsky YZ, Yaakov Y, Assayag M, *et al.* Preconditioning allows engraftment of mouse and human embryonic lung cells, enabling lung repair in mice. *Nat Med* **2015**; 21: 869-79. https://doi.org/10.1038/nm.3889
3. Nikolić MZ, Caritg O, Jeng Q, Johnson JA, Sun D, Howell KJ, *et al.* Human embryonic lung epithelial tips are multipotent progenitors that can be expanded in vitro as long-term self-renewing organoids. *eLife* **2017**; 6: e26575. https://doi.org/10.7554/elife.26575.059
4. Nikolic MZ, Sun D, Rawlins EL. Human lung development: recent progress and new challenges. *Development* **2018**; 145. https://doi.org/10.1242/dev.163485
5. Danopoulos S, Alonso I, Thornton ME, Grubbs BH, Bellusci S, Warburton D, *et al.* Human lung branching morphogenesis is orchestrated by the spatiotemporal distribution of ACTA2, SOX2, and SOX9. *Am J Physiol Lung Cell Mol Physiol* **2018**; 314: L144-L9. https://doi.org/10.1152/ajplung.00379.2017
6. Mishra R, Benlhabib H, Guo W, Lerma Cervantes CB, Mendelson CR. Developmental decline in the MicroRNA 199a (miR-199a)/miR-214 cluster in human fetal lung promotes type II cell differentiation by upregulating key transcription factors. *Mol Cell Biol* **2018**; 38. https://doi.org/10.1128/mcb.00037-18
7. Miller AJ, Yu Q, Czerwinski M, Tsai YH, Conway RF, Wu A, *et al.* In vitro and in vivo development of the human airway at single-cell resolution. *Dev Cell* **2020**; 53: 117-28.e6. https://doi.org/10.1016/j.devcel.2020.01.033
8. Herriges M, Morrisey EE. Lung development: orchestrating the generation and regeneration of a complex organ. *Development*

**2014**; 141: 502-13. https://doi.org/10.1242/dev.098186
9. Tzouvelekis A, Toonkel R, Karampitsakos T, Medapalli K, Ninou I, Aidinis V, *et al.* Mesenchymal Stem Cells for the Treatment of Idiopathic Pulmonary Fibrosis. *Front Med (Lausanne)* **2018**; 5: 142. https://doi.org/10.3389/fmed.2018.00142
10. Hashimoto N, Jin H, Liu T, Chensue SW, Phan SH. Bone marrow-derived progenitor cells in pulmonary fibrosis. *J Clin Invest* **2004**; 113: 243-52. https://doi.org/10.1172/jci18847
11. Serrano-Mollar A, Nacher M, Gay-Jordi G, Closa D, Xaubet A, Bulbena O. Intratracheal transplantation of alveolar type II cells reverses bleomycin-induced lung fibrosis. *Am J Respir Crit Care Med* **2007**; 176: 1261-8. https://doi.org/10.1164/rccm.200610-1491OC
12. Lim R, Chan ST, Tan JL, Mockler JC, Murphy SV, Wallace EM. Preterm human amnion epithelial cells have limited reparative potential. *Placenta* **2013**; 34: 486-92. https://doi.org/10.1016/j.placenta.2013.03.010
13. Hern WM. Correlation of fetal age and measurements between 10 and 26 weeks of gestation. *Obstet Gynecol* **1984**; 63: 26-32.
14. Abe S, Yamamoto M, Noguchi T, Yoshimoto T, Kinoshita H, Matsunaga S, *et al.* Fetal development of the minor lung segment. *Anat Cell Biol* **2014**; 47: 12-7. https://doi.org/10.5115/acb.2014.47.1.12
15. Ashcroft T, Simpson JM, Timbrell V. Simple method of estimating severity of pulmonary fibrosis on a numerical scale. *J Clin Pathol* **1988**; 41: 467-70. https://doi.org/10.1136/jcp.41.4.467
16. Smirnova NF, Schamberger AC, Nayakanti S, Hatz R, Behr J, Eickelberg O. Detection and quantification of epithelial progenitor cell populations in human healthy and IPF lungs. *Respir Res* **2016**; 17: 83. https://doi.org/10.1186/s12931-016-0404-x
17. Ghosh M, Ahmad S, Jian A, Li B, Smith RW, Helm KM, *et al.* Human tracheobronchial basal cells. Normal versus remodeling/repairing phenotypes in vivo and in vitro. *Am J Respir Cell Mol Biol* **2013**; 49: 1127-34. https://doi.org/10.1165/rcmb.2013-0049OC
18. Kreda SM, Gynn MC, Fenstermacher DA, Boucher RC, Gabriel SE. Expression and localization of epithelial aquaporins in the adult human lung. *Am J Respir Cell Mol Biol* **2001**; 24: 224-34. https://doi.org/10.1165/ajrcmb.24.3.4367
19. Avril-Delplanque A, Casal I, Castillon N, Hinnrasky J, Puchelle E, Péault B. Aquaporin-3 expression in human fetal airway epithelial progenitor cells. *Stem Cells* **2005**; 23: 992-1001. https://doi.org/10.1634/stemcells.2004-0197
20. Khoor A, Stahlman MT, Gray ME, Whitsett JA. Temporal-spatial distribution of SP-B and SP-C proteins and mRNAs in developing respiratory epithelium of human lung. *J Histochem Cytochem* **1994**; 42: 1187-99. https://doi.org/10.1177/42.9.8064126
21. Solarin KO, Ballard PL, Guttentag SH, Lomax CA, Beers MF. Expression and glucocorticoid regulation of surfactant protein C in human fetal lung. *Pediatr Res* **1997**; 42: 356-64. https://doi.org/10.1203/00006450-199709000-00017
22. Miskovic J, Brekalo Z, Vukojevic K, Miskovic HR, Kraljevic D, Todorovic J, *et al.* Co-expression of TTF-1 and neuroendocrine markers in the human fetal lung and pulmonary neuroendocrine tumors. *Acta Histochem* **2015**; 117: 451-9. https://doi.org/10.1016/j.acthis.2015.02.002
23. Tanaka Y, Yamaguchi M, Hirai S, Sumi T, Tada M, Saito A, *et al.* Characterization of distal airway stem-like cells expressing N-terminally truncated p63 and thyroid transcription factor-1 in the human lung. *Exp Cell Res* **2018**; 372: 141-9. https://doi.org/10.1016/j.yexcr.2018.09.020
24. Shirani A, Ganji F, Golmohammadi M, Hashemi SM, Mozafari M, Amoabediny G, *et al.* Cross-linked acellular lung for application in tissue engineering: Effects on biocompatibility, mechanical properties and immunological responses. *Mater Sci Eng C Mater Biol Appl* **2021**; 122: 111938. https://doi.org/10.1016/j.msec.2021.111938
25. Juul NH, Stockman CA, Desai TJ. Niche Cells and Signals that Regulate Lung Alveolar Stem Cells In Vivo. *Cold Spring Harbor perspectives in biology* **2020**; 12. https://doi.org/10.1101/cshperspect.a035717
26. Mondrinos MJ, Jones PL, Finck CM, Lelkes PI. Engineering de novo assembly of fetal pulmonary organoids. *Tissue Eng Part A* **2014**; 20: 2892-907. https://doi.org/10.1089/ten.tea.2014.0085
27. Strikoudis A, Cieślak A, Loffredo L, Chen YW, Patel N, Saqi A, *et al.* Modeling of Fibrotic Lung Disease Using 3D Organoids Derived from Human Pluripotent Stem Cells. *Cell Rep* **2019**; 27: 3709-23 e5. https://doi.org/10.1016/j.celrep.2019.05.077
28. Khalil N, Parekh TV, O'Connor RN, Gold LI. Differential expression of transforming growth factor-beta type I and II receptors by pulmonary cells in bleomycin-induced lung injury: correlation with repair and fibrosis. *Exp Lung Res* **2002**; 28: 233-50. https://doi.org/10.1080/019021402753570527
29. García-Prieto E, González-López A, Cabrera S, Astudillo A, Gutiérrez-Fernández A, Fanjul-Fernandez M, *et al.* Resistance to bleomycin-induced lung fibrosis in MMP-8 deficient mice is mediated by interleukin-10. *PloS One* **2010**; 5: e13242. https://doi.org/10.1371/journal.pone.0013242
30. Shamskhou EA, Kratochvil MJ, Orcholski ME, Nagy N, Kaber G, Steen E, *et al.* Hydrogel-based delivery of Il-10 improves treatment of bleomycin-induced lung fibrosis in mice. *Biomaterials* **2019**; 203: 52-62. https://doi.org/10.1016/j.biomaterials.2019.02.017
31. Guo L, Karoubi G, Duchesneau P, Aoki FG, Shutova MV, Rogers I, *et al.* Interrupted reprogramming of alveolar type II cells induces progenitor-like cells that ameliorate pulmonary fibrosis. *NPJ Regen Med* **2018**; 3: 14. https://doi.org/10.1038/s41536-018-0052-5